

Dynamic generation of GHZ states of three coupled charge qubits

J. Nogueira,¹ P. A. Oliveira,^{2,1} F. M. Souza,¹ and L. Sanz¹

¹*Instituto de Física, Universidade Federal de Uberlândia, Av. João Naves de Ávila, 2121 - Santa Mônica, Uberlândia - MG, 38408-100, Brazil*

²*Instituto Federal Goiano, Campus Catalão, 75701-655, Catalão, GO, Brazil*

(Dated: March 11, 2022)

In this paper, we present a proof-of-principle of the formation of pure maximally entangled states from the Greenberger-Horne-Zeilinger class for three-qubits, in the experimental context of charged quantum dots. Each qubit must be identified as a pair of quantum dots coupled through a tunneling parameter, that allows electron tunneling between the dots. The Coulomb interaction is accounted for and is responsible for the coupling between the qubits. The interplay between coherent tunneling events and many-body interaction gives rise to the formation of highly entangled states. An effective model sheds light on the role of a third-order tunneling process behind the dynamics, and the action of charge dephasing is quantified in the process.

I. INTRODUCTION

Since the rise of the research on quantum information at the end of the XX century [1, 2], semiconductor nanostructures have been pointed out as an interesting platform for the experimental implementation of quantum information processing. After twenty years, these at first theoretical expectations has been gradually fulfilled, with successful experimental realizations as the recent implementation of the fastest two-qubit gate using a 2D electronic gas in silicon [3, 4]. Although electron spin 1/2 states are the most common system to encode qubits [5], semiconductors offer other possibilities as the electronic state qubits defined in charged quantum dots [6, 7], the singlet-triplet qubit states of two-electrons in GaAs [8, 9], and the exchange-only qubit with spin states [10], among others.

Quantum Dots (QDs) have been defined as artificial atoms, once the spatial confinement favors the formation of a discrete spectrum of electronic levels [11]. From all the possibilities of encoding a qubit, as in the excitonic states [12–14] and the electronic spin [15, 16], the interest on the physics of charged quantum dots has been increasing, once they are scalable systems where initialization and readout are possible through a process involving detection even of a single electron [17, 18]. In this physical system, the qubits are defined based on the property of electronic tunneling [7, 19], with the single-qubit operations being controlled by external gate voltages [7, 19]. Moreover, the single-molecule electronics has been an outstanding new field of research, due to its future feasible implementations as the construction of a cheaper and faster single-electron transistor [20, 21].

In this work, we investigate a system composed of three charge qubits, each qubit consisting of a pair of quantum dots that form a quantum molecule. The qubit is encoded in one electron in excess, that coherently tunneled between the dots. Electrons from separate quantum molecules interact by Coulomb electrostatic interaction, which couples the qubits. Our main goal is to establish physical conditions for the generation of gen-

uine multipartite maximally entangled states, belonging to the GHZ class. This is the first step in the exploration of the scalability of this particular system, in front of the results for the case of two charge qubits [22–24]. We are interested not only in explore, by numerical simulations, this dynamic, but also in the comprehension of the specific process behind the formation of the states and the feasibility of the proposal, in terms of the effects of the decoherence process due to charge dephasing. Proposals of a generation of the W states, another tripartite entangled state, had been studied recently in the context of spin-qubits [16] and superconductor qubits [25]. As far as we know, this is the first theoretical demonstration that many-body interactions yields to highly entangled GHZ states in semiconductor charged quantum dots.

This paper is organized as follows. In section II, we present the model used to describe our system of interest, introducing the Hamiltonian operator for the physical setup and then showing the conditions for encoding the three qubits. We also present some entanglement quantifiers that will be used for the characterization of the GHZ-class states. Section III is devoted to the presentation of our main results: the numerical simulations for the generation of GHZ states together with the discussion about an effective two-level hamiltonian which illustrates how a three-order tunneling process explains the formation of the target states. The action of charge dephasing, the main mechanism of decoherence in our system of interest, is discussed in Sec. IV, and Sec. V contains our final remarks.

II. MODEL AND ENTANGLEMENT QUANTIFIERS

In this section, we present the physical system considered, its model Hamiltonian, and a summary of the entanglement quantifiers. Our model consists of a three-qubit system, codified in charged quantum dots. Each qubit is encoded in the electronic states of a double dot molecular structure [6]. By attaching particle reservoirs to the molecules, the system can be initialized in a con-

figuration of charge, on demand. Additionally, Coulomb interaction between molecules is considered at least for first neighbors [7, 26]. This kind of multiple dots structure has been experimentally explored in the last two decades [27, 28].

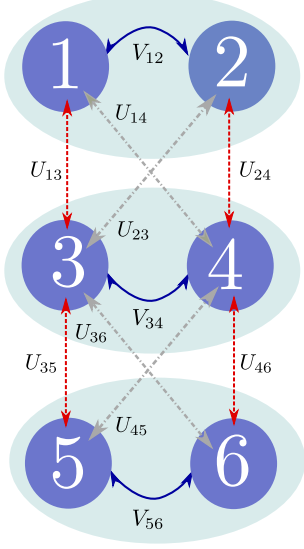


FIG. 1. (Color online) Sketch of the physical system: six quantum dots are coupled by pairs, each pair being a quantum molecule. Electronic coherent tunneling are permitted inside each molecule, although is forbidden between dots belonging to different molecules. The allowed tunneling couplings are shown with blue solid lines. Electrostatic coupling permits the interaction between electrons in different molecules, and are indicated by dot and dashed dot lines.

A sketch of the physical system is shown in Fig. 1. The six quantum dots are actually built at the intersection of two semiconductors of different band gaps (e.g. GaAs/AlGaAs), which sustains a two-dimensional electron gas (2DEG). The QDs are then delimited by spatial confinement obtained by the action of negative biased voltages on gate electrodes at the top of the 2DEG. Additionally, some extra gates couple the system with electronic reservoirs (not shown in the scheme): a source provides electrons to enter in the system and a drain withdraw charges, in a process that permits, for example, measurements of the current through each qubit. Extra electrodes attached at various points of the system are also used to attain a fine control of the physical parameters of tunneling, V_{ij} , and electronic energies, E_i , by simply varying gate voltages [6, 7, 27, 29].

We consider a closed system that is already initialized in one of the eight possible states for three qubits. We assume that the system is in the Coulomb blockade regime, where only a single electron per qubit is allowed. Our model Hamiltonian is written in second quantization as

$$\hat{H}_{6\text{QDs}} = \sum_{i=1}^6 E_i \hat{n}_i + \hat{V} + \hat{U}, \quad (1)$$

where

$$\hat{V} = V_{12} \hat{d}_1^\dagger \hat{d}_2 + V_{34} \hat{d}_3^\dagger \hat{d}_4 + V_{56} \hat{d}_5^\dagger \hat{d}_6 + \text{h.c.} \quad (2)$$

$$\begin{aligned} \hat{U} = & U_{13} \hat{n}_1 \hat{n}_3 + U_{14} \hat{n}_1 \hat{n}_4 + U_{23} \hat{n}_2 \hat{n}_3 + U_{24} \hat{n}_2 \hat{n}_4 \\ & + U_{35} \hat{n}_3 \hat{n}_5 + U_{36} \hat{n}_3 \hat{n}_6 + U_{45} \hat{n}_4 \hat{n}_5 + U_{46} \hat{n}_4 \hat{n}_6, \end{aligned} \quad (3)$$

with \hat{d}_i^\dagger (\hat{d}_i) being the fermionic creation (annihilation) operator, and $\hat{n}_i = \hat{d}_i^\dagger \hat{d}_i$ is the number operator to the i th dot. The first term in Eq. (1) is the energy of the electronic level in each dot. The second, given by Eq. (2), describes the intra molecule tunnel coupling, while the last term, Eq.(3), accounts for the Coulomb interaction between molecules.

The Hilbert space $\mathcal{H}_{6\text{QDs}}$ of the system is a 64-dimensional space with elements being $\{|1\rangle^{\otimes 6}, \dots, |0\rangle^{\otimes 6}\}$, and $|1\rangle$ ($|0\rangle$) standing for the dot being occupied (empty). Imposing the condition when a single electron per qubit is considered, the accessible Hilbert reduces to only 8 states, with each molecule occupying one of the states $|10\rangle$ or $|01\rangle$. Defining $|10\rangle = |0\rangle$ and $|01\rangle = |1\rangle$, the complete basis turns out to be $\{|000\rangle, |001\rangle, |010\rangle, |011\rangle, |100\rangle, |101\rangle, |110\rangle, |111\rangle\}$, with the Hamiltonian expressed as

$$\hat{H}_{3\text{qb}} = \sum_{q=1}^3 [\varepsilon_q \hat{\sigma}_z^{(q)} + \Delta_q \hat{\sigma}_x^{(q)}] + \sum_{q',q''} J_{q'q''} \hat{\sigma}_z^{(q')} \otimes \hat{\sigma}_z^{(q'')}, \quad (4)$$

where $\sigma_z = |0\rangle \langle 0| - |1\rangle \langle 1|$, and $\sigma_x = |0\rangle \langle 1| + |1\rangle \langle 0|$. Here, the index $q = 1, 2, 3$ denotes the qubits in the first two terms while $q' = 1, 2$ with $q'' = q' + 1$ are used in the third term. The first term describes the detuning of the electronic energies for each qubit, the second gives the tunneling process inside each qubit, and the third term provides the Coulomb interaction between qubits. We also use a new physical parametrization where $2\varepsilon_j$ is the detuning between the electronic levels of each dot inside the j th molecule, Δ_j is the tunneling parameter, and parameters $J_{q'q''}$ take into account the Coulomb interactions between electrons in different qubits. Notice that this Hamiltonian is an extension of the case for a two-qubit system in the context of charged quantum dots studied in earlier works [22–24].

As the number of qubits encoded in a quantum system increases, to determine the entanglement degree of quantum states becomes a challenge. To the well-known case of a two-qubit system, one can easily characterize the physical states as being separable or entangled. A similar analysis is not that simple for the case of three qubits [30–32]. Apart from the fully separable states, there are three classes of entangled states. We can say that two different entangled states belong to the same equivalence class if it is possible to find a set of Stochastic Local Operations and Classical Communication (SLOCC) that transform one state into another, with non null probability of success. Thus, concerning the classes of entangled states for three qubits, the first is the class of biseparable states, where one qubit remains separate while the

rest two qubits show bipartite entanglement. The second and the third classes, the W and GHZ states, are two different families that show genuine tripartite entangled states [31].

We are interested in the dynamical formation of states belonging to the GHZ class. The representant for elements from this class can be written as

$$|\Psi_{\text{GHZ}}(\phi)\rangle = \frac{1}{\sqrt{2}} (|000\rangle + e^{i\phi} |111\rangle), \quad (5)$$

where ϕ is a relative phase. Notice that the application of the operator $I \otimes \sigma_x \otimes I$ on $|\Psi_{\text{GHZ}}\rangle$ results in a new state of the form

$$|\Psi_{\text{FLIP}}(\phi)\rangle = \frac{1}{\sqrt{2}} (|010\rangle + e^{i\phi} |101\rangle), \quad (6)$$

which belongs to the same GHZ class, once the operation is an invertible local operator (ILO). This means that the states in Eqs. (5)-(6) are SLOCC equivalent. In what follows, we will focus on the formation of both GHZ and FLIP states.

In order to characterize the dynamical formation of GHZ states, we calculate both, the fidelity (\mathcal{F}) and the 3-tangle (τ_3), a useful entanglement quantifier for the GHZ class [33]. The first is defined as

$$\mathcal{F} = \text{Tr} [\hat{\rho}(t) \hat{\rho}_{\text{target}}], \quad (7)$$

which reaches 1 as the evolved density matrix operator, $\hat{\rho}(t)$, approaches to the target state $\hat{\rho}_{\text{target}}$. The second is defined as

$$\tau_3 = \tau_{A(BC)} - \tau_{AB} - \tau_{AC}, \quad (8)$$

with A, B, and C representing three qubits, and

$$\tau_{A(BC)} = 4\text{Det}(\hat{\rho}_A), \quad (9)$$

where $\hat{\rho}_A$ is the reduced density operator obtained by taken the partial trace with respect to both B and C qubits, i.e., $\hat{\rho}_A = \text{Tr}_B\{\text{Tr}_C\{\hat{\rho}(t)\}\}$. For the calculation of τ_3 it is necessary to calculate

$$\tau_{AB} = \text{Tr}(\hat{\rho}_{AB} \tilde{\hat{\rho}}_{AB}) - 2\lambda_1\lambda_2, \quad (10)$$

where $\hat{\rho}_{AB} = \text{Tr}_C\{\hat{\rho}(t)\}$, $\tilde{\hat{\rho}}_{AB} = (\hat{\sigma}_y \otimes \hat{\sigma}_y) \hat{\rho}_{AB}^* (\hat{\sigma}_y \otimes \hat{\sigma}_y)$ being the spin-flip density operator, and $\hat{\rho}_{AB}^*$ is the complex conjugate of $\hat{\rho}_{AB}$. The values λ_1 and λ_2 are the only non-null square root eigenvalues of the operator $\hat{\rho}_{AB} \tilde{\hat{\rho}}_{AB}$. A similar definition holds for τ_{AC} .

As an auxiliary quantity, we define

$$\tau_2 = \tau_{AB} + \tau_{AC}, \quad (11)$$

which quantifies the amount of bipartite entanglement in the three qubit system. This entanglement quantifier is used in our numerical calculations to establish if some pure state $\hat{\rho}(t)$ belongs to the GHZ class of entangled states, with a 3-tangle value reaching $\tau_3[\hat{\rho}(t)] = 1$ while $\tau_2 = 0$, showing genuine multipartite entanglement.

III. DYNAMICAL GENERATION OF GHZ STATES

In this section we discuss the main results of our work, being the dynamical generation of a state with genuine multipartite entanglement, belonging to the GHZ class. The dynamics of the closed system is obtained by solving the Von Neumann equation for the density matrix operator $\hat{\rho}(t)$ ($\hbar = 1$),

$$\dot{\hat{\rho}}(t) = -i[\hat{H}_{\text{3qb}}, \hat{\rho}]. \quad (12)$$

Once the evolved density matrix $\hat{\rho}(t)$ is obtained, we calculate the population of states $|000\rangle$ and $|111\rangle$ via

$$P_e(t) = \text{Tr} [\hat{\rho}(t) \hat{\rho}_e], \quad (13)$$

where $\hat{\rho}_e = |e\rangle \langle e|$ with $e = 000$ or 111 . We also calculate the entanglement measurements defined in Sec. II, and the fidelity, choosing some target state from the GHZ class, considering a specific value of relative phase ϕ in Eq. (5).

In our simulations, the Coulomb strength is fixed at $J_{12} = J_{23} = J = 25\mu\text{eV}$ [26], and we set all physical parameters in Hamiltonian (4) in terms of J . A preliminar numerical analysis of the dynamics shows that the best conditions for the generation of a GHZ state occurs when the electronic levels are resonant ($\varepsilon_1 = \varepsilon_2 = \varepsilon_3 = 0$), and the molecules has equal tunneling couplings being $\Delta_1 = \Delta_2 = \Delta_3 = \Delta$. In order to choose one specific value of Δ , we run simulations looking for a combination of both, low times for formation of the GHZ state and high fidelity. In the range of $J/10 \leq \Delta \leq J/2$, the numerical estimation of the time of formation of a GHZ state falls from 20 ns to 0.1 ns. At the same times, high values of Δ shows a decrease of the fidelity of evolved state with a GHZ target state, from 0.99 to 0.91. In order to keep both, short times of formation, important in order to face processes of decoherence, and high fidelity, we chose $\Delta = J/6$ for the illustration of our proof-of-principle of generation of GHZ states.

Figure 2(a) shows both $P_{000}(t)$ and $P_{111}(t)$ against $\Omega_{\text{GHZ}} t$, considering $\hat{\rho}(0) = |000\rangle \langle 000|$ as the initial condition. The choice of the frequency Ω_{GHZ} to parametrize the temporal evolution will be made clear soon. Notice that when $P_{000} = P_{111} = 0.5$ at $\Omega_{\text{GHZ}} t'_{\text{GHZ}} \approx \pi/4$, we obtain a highly entangled state, according to $\tau_3 = 1$, shown by the black squares in Fig. 2(b). For this particular time we also find $\tau_2 = 0$ (not shown here) [34]. To confirm the formation of GHZ states given by Eq.(5), we calculate the fidelities $\mathcal{F}_{\text{GHZ}_-}$ (brown filled triangles), and $\mathcal{F}_{\text{GHZ}_+}$ (brown crosses), which correspond to target states with $\phi = -\pi/2$ and $\phi = \pi/2$ in Eq.(5), respectively. Once, at time t'_{GHZ} , the fidelity $\mathcal{F}_{\text{GHZ}_-}$ becomes close to one, these results allow us to conclude that, at this particular time, the evolved state is given by

$$|\Psi(t'_{\text{GHZ}})\rangle \approx |\Psi_{\text{GHZ}}(-\pi/2)\rangle = \frac{1}{\sqrt{2}} (|000\rangle - i|111\rangle). \quad (14)$$

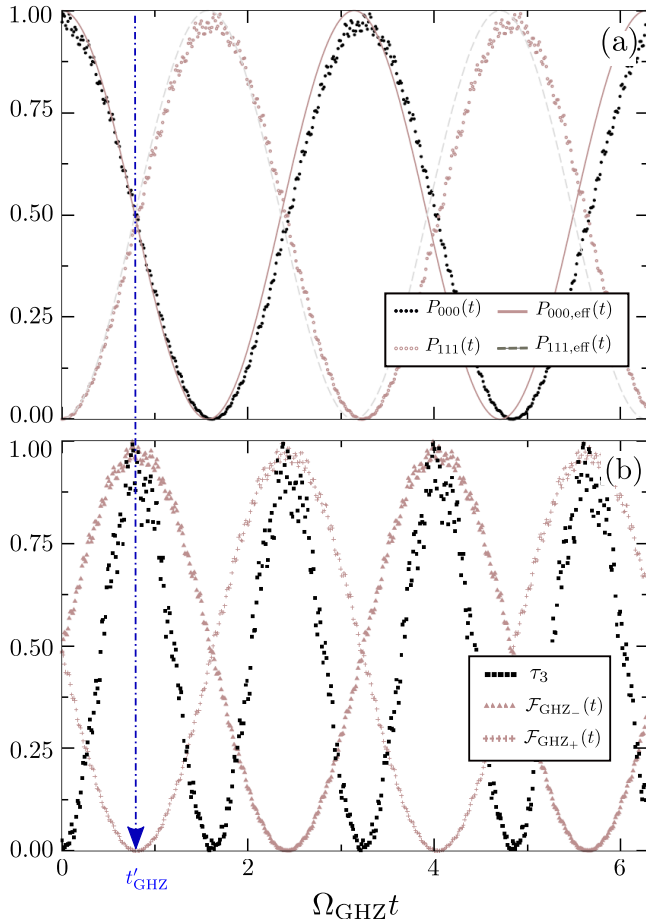


FIG. 2. (Color online) Quantum electronic dynamics in three quantum molecules, as a function of the dimensionless parameter $\Omega_{\text{GHZ}}t$ considering the initial condition $\hat{\rho}(0) = |000\rangle\langle 000|$, and physical parameters given by $\varepsilon_i = 0$, $J = 25\mu\text{eV}$ and $\Delta = J/6$ in the Hamiltonian, Eq.(4). Panel (a) shows the populations $P_{000}(t)$ (black dots) and $P_{111}(t)$ (brown open circles), together with the evolution of the same quantities considering the effective two-level system as discussed in Sec. III: $P_{000,\text{eff}}(t)$ (brown solid line) and $P_{111,\text{eff}}(t)$ (gray dashed line). Panel (b): Evolution of the entanglement quantifier τ_3 (black squares), and the fidelities $\mathcal{F}_{\text{GHZ}-}(t)$ (brown filled triangles), and $\mathcal{F}_{\text{GHZ}+}(t)$ (brown crosses). The blue dashed-dot line shows the time of formation of the first GHZ state, corresponding to $t'_{\text{GHZ}} = 4.56$ ns as predicted by the effective two-level model.

Also in Fig. 2(b), we find $\mathcal{F}_{\text{GHZ}+}$ close to one, for $\Omega_{\text{GHZ}}t \approx 3\pi/4$, thus revealing the formation of $|\Psi_{\text{GHZ}}(\pi/2)\rangle$. With the same choice of physical parameters but considering the initial condition $\hat{\rho}(0) = |010\rangle\langle 010|$, we observe a similar behavior behind the formation of FLIP states (see Appendix A for details). It is valid that, for the experimental value of $J = 25\mu\text{eV}$, the earliest time of generation of a GHZ is around $t'_{\text{GHZ}} \approx 4.5$ ns.

Let us search for a two-level model which will provide an important insight on the generation of the GHZ states. We start rewriting the three-qubit Hamiltonian

from Eq. (4) as

$$\hat{H}_{3\text{qb}} = \hat{H}_0 + \hat{V},$$

where

$$\hat{H}_0 = \sum_{q=1}^3 \varepsilon_q \hat{\sigma}_z^{(q)} + \sum_{q',q''} J_{q'q''} \hat{\sigma}_z^{(q')} \otimes \hat{\sigma}_z^{(q'')}, \quad (15)$$

is the diagonal term of the Hamiltonian. The energies E_k^0 of \hat{H}_0 can be expressed as

$$E_{000}^0 = E_{111}^0 = 2J, \quad (16)$$

$$E_{010}^0 = E_{101}^0 = -2J, \quad (17)$$

$$E_{001}^0 = E_{011}^0 = E_{100}^0 = E_{110}^0 = 0, \quad (18)$$

obtained from Eqs.(B1) in Appendix B, with $\varepsilon_q = 0$ for all values of q , and $J_{12} = J_{23} = J$. As discussed also in Appendix B, at this condition there are three subspaces well energetically separated (by a gap $|2J|$) from each other, i.e., the subspace spanned by $\{|000\rangle, |111\rangle\}$, the one given by $\{|010\rangle, |101\rangle\}$ and finally the largest one with $\{|001\rangle, |011\rangle, |100\rangle, |110\rangle\}$.

The non-diagonal term of $\hat{H}_{3\text{qb}}$

$$\hat{V} = \Delta \sum_{i=1}^3 \hat{\sigma}_x^i, \quad (19)$$

describes the action of tunneling. This coupling removes energy degeneracies of \hat{H}_0 inside each subspace. For $\Delta < J/4$, numerical calculations show that the eigenstates from the original subspace with $E = 2J$ become GHZ states with $\phi = 0$ and $\phi = \pi$ in Eq.(5)(see Appendix B for details).

At this point, we consider the tunneling coupling as a perturbation, in order to find an analytical expression for the effective two-level coupling, following a procedure used in a recent work [22]. As we are interested in the formation of the GHZ state given by Eq. (5), we can assume that the system is initialized in one of the states $|000\rangle$ or $|111\rangle$. Since no relaxation mechanisms are present (charge dephasing will be accounted for in the next section), we expect a temporal evolution from the initial state to a coherent superposition of both, $|000\rangle$ and $|111\rangle$ states. However, no direct coupling between these two states is present. In order to undergo a quantum evolution inside this subspace, the system needs to perform virtual transitions via the other states of the three-qubit basis. This virtual mechanism can be explained via perturbation theory.

The calculation involves separate the original basis of three-qubits in two parts, where A is a two-dimensional subspace with elements $|000\rangle$ and $|111\rangle$ and B contains the remaining six elements. The matrix representation of the Hamiltonian which describes the problem can be seen as

$$\tilde{H} = \hat{H}_0 + \hat{V} = \begin{pmatrix} \tilde{\hat{H}}^{AA} & \tilde{\hat{H}}^{AB} \\ \tilde{\hat{H}}^{BA} & \tilde{\hat{H}}^{BB} \end{pmatrix}. \quad (20)$$

Following the steps detailed in the Appendix C, we arrive to a two-level effective hamiltonian written as

$$\hat{H}_{\text{eff}}^{\text{GHZ}} = \Omega_{\text{GHZ}} |111\rangle\langle 000| + h.c., \quad (21)$$

where Ω_{GHZ} corresponds to

$$\Omega_{\text{GHZ}} = \sum_{k=1}^8 \sum_{u=1}^8 \langle 111 | \tilde{H}^{AB} | k \rangle \langle k | (E - \tilde{H}_0^{BB})^{-1} \hat{V}^{BB} \times (E - \tilde{H}_0^{BB})^{-1} | u \rangle \langle u | \tilde{H}^{BA} | 000 \rangle. \quad (22)$$

Here the indexes k and u run over all the states in the computational basis, and \hat{V}^{BB} is the 6×6 matrix representation of the perturbation \hat{V} in the subspace B . Notice that the sequence of the operators \tilde{H}^{AB} , \hat{V}^{BB} , and \tilde{H}^{BA} in the numerator of Eq. (22) indicate that third-order processes are behind the emergence of anticrossing of $|000\rangle$ and $|111\rangle$. Expanding the sum and substituting the matrix elements, the expression becomes

$$\Omega_{\text{GHZ}} = \Delta^3 \left[\frac{1}{E_A - E_{011}} \left(\frac{1}{E_A - E_{001}} + \frac{1}{E_A - E_{010}} \right) + \frac{1}{E_A - E_{101}} \left(\frac{1}{E_A - E_{001}} + \frac{1}{E_A - E_{100}} \right) + \frac{1}{E_A - E_{110}} \left(\frac{1}{E_A - E_{010}} + \frac{1}{E_A - E_{100}} \right) \right]. \quad (23)$$

The term E_A in the equation can be approximated as the eigenenergy of the unperturbed Hamiltonian \tilde{H}_0 in the subspace A , which is $E_A = 2J$ (or $E_A = -2J$, when describing the dynamics inside the FLIP space). Finally, we arrive to the expression of the effective coupling (in units of energy)

$$\Omega_{\text{GHZ}} = \frac{\Delta^3}{J^2}. \quad (24)$$

By using the Eq. (24) inside Eq. (21) and calculating the quantum dynamics, we obtain the Rabi oscillations for the effective populations $P_{000,\text{eff}}(t)$ (brown solid line) and $P_{111,\text{eff}}(t)$ (gray dashed line), plotted in Fig. 2. Notice that the model describes well the results of the exact calculation at short times. A similar behavior can be observed for the dynamics considering an initial condition for the formation of FLIP states, as shown in Fig. 4 in Appendix A. From our numerical calculations, we see that the quantum dynamics do not behave as periodic and show ripples, both signs of a more complex dynamics, which involves the whole set of eight states on the unitary dynamics. Still, at short times and small tunneling rates, the effective model becomes a useful tool for the estimation of the value of the time of formation of GHZ state, which is

$$t'_{\text{GHZ}} = \frac{\pi}{4} \frac{J^2}{\Delta^3}. \quad (25)$$

With this expression, we estimate $t'_{\text{GHZ}} = 4.56\text{ns}$ for the physical conditions in Fig. 2. This time scale is shown

in the figure with the blue dashed-dot line, coinciding with the formation of the state $|\Psi_{\text{GHZ}}(-\pi/2)\rangle$. Following the same procedure, but considering the two-level system with energies $E = -2J$ as A , we arrive to an equivalent expression but the case of formation of FLIP states. The final result gives $\Omega_{\text{FLIP}} = \Omega_{\text{GHZ}}$, thus explaining the similarities between the dynamics of the two cases, as observed by comparing Fig. 2 and Fig. 4 (Appendix A).

IV. DYNAMICAL BEHAVIOR UNDER A DEPHASING CHANNEL

In this section we discuss the effects of charge dephasing, the main decoherence process in the context of charged quantum dots [35–37]. To quantify the effect of dephasing on the generation of a GHZ state, we numerically solve a Lindblad master equation [26] written as

$$\dot{\rho}(t) = -i[\hat{H}_{3\text{qb}}, \hat{\rho}] + \frac{1}{2} \sum_{k=1}^8 \Gamma_k \left(2\hat{L}_k \hat{\rho} \hat{L}_k^\dagger - \hat{L}_k \hat{L}_k^\dagger \hat{\rho} - \hat{\rho} \hat{L}_k \hat{L}_k^\dagger \right), \quad (26)$$

where the Γ_k are the rates associated with the dephasing channel in energy units, \hat{L}_k are the jump operators, and the time scale of the dephasing process is given by $T_{\text{deph}} = 1/\gamma_k = h/\Gamma_k$, with γ_k in Hertz. The physical agent behind this process is the background charge fluctuation. To model the effect of dephasing, we consider the operators

$$\hat{L}_k = |k\rangle\langle k|, \quad (27)$$

in Eq. (26). Here $|k\rangle$ is one of the elements of the computational basis where $\hat{L}_1 = |000\rangle\langle 000|$, $\hat{L}_2 = |001\rangle\langle 001|$, and so on. We run our numerical simulation in order to solve the master equation (26) considering $\Gamma_k = \Gamma_{\text{deph}}$ for all k .

In Fig. 3, we plot our results for the dynamics of populations $P_{000}(t)$ (black dots) and $P_{111}(t)$ (brown open circles), and the fidelity $\mathcal{F}_{\text{GHZ}_-}$ (brown triangles), considering three different values of dephasing parameters: $\gamma_{\text{deph}} = 10^{-2}$ GHz in panel (a), $\gamma_{\text{deph}} = 10^{-1}$ GHz in panel (b), and $\gamma_{\text{deph}} = 1$ GHz in panel (c). The physical parameters are the same than in Fig. 2. We focus on the formation of the GHZ state $|\Psi_{\text{GHZ}}(-\pi/2)\rangle$ once this state is generated earlier in the dynamics. The results show the high sensibility of the three qubit dynamics over this process. Even for small rates of dephasing, Fig. 3(a), the decreasing amplitude of oscillations is a clear sign that the process promotes population to others accessible states in a incoherent evolution. At t'_{GHZ} , we still have the maximum for the fidelity with value $\mathcal{F}_{\text{GHZ}_-} \approx 0.85$ for the target state $|\Psi_{\text{GHZ}}(-\pi/2)\rangle$, although the populations at this time show a higher value for P_{000} (around 0.62), which means the dephasing process affects strongly the third-order tunneling processes behind the effective two-level dynamics for the formation

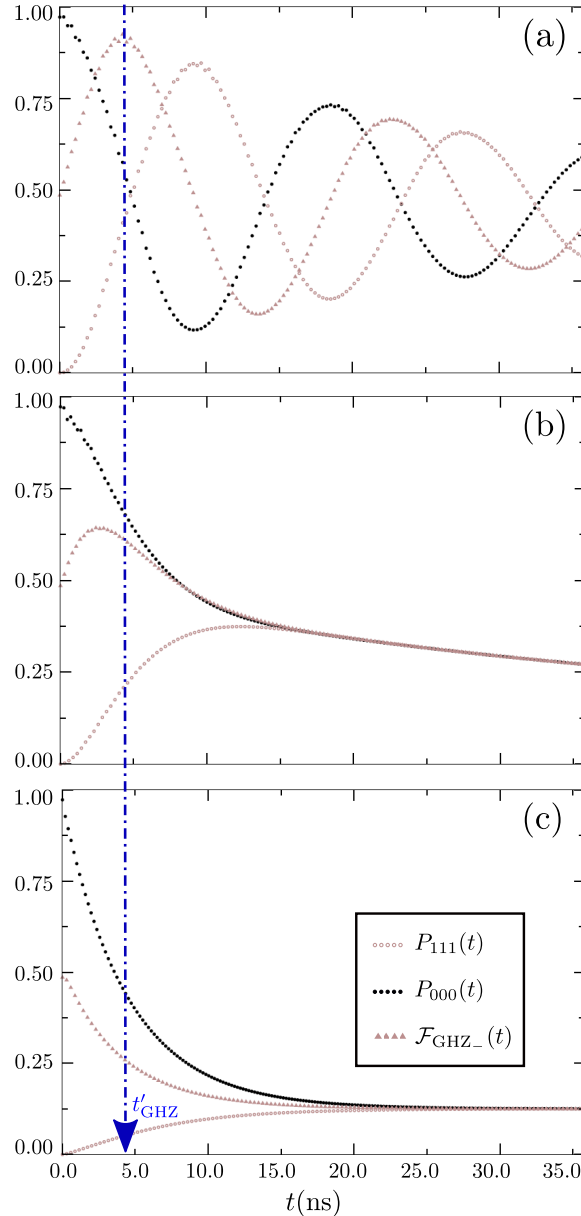


FIG. 3. (Color online) Dynamics of populations $P_{000}(t)$ (black dots) and $P_{111}(t)$ (brown open circles), as well as the fidelity $\mathcal{F}_{\text{GHZ-}}$ (brown triangles) considering the action of the dephasing for $\varepsilon_i = 0$, $J = 25\mu\text{eV}$, $\Delta = J/6$, and the initial condition $\hat{\rho}(0) = |000\rangle\langle 000|$ with (a) $\gamma_{\text{deph}} = 10^{-2}$ GHz; (b) $\gamma_{\text{deph}} = 10^{-1}$ GHz, and (c) $\gamma_{\text{deph}} = 1$ GHz. The blue dashed-dot line shows the time of formation of the first GHZ state, corresponding to $t'_{\text{GHZ}} \approx 4.46$ ns.

of the GHZ-class states. Increasing the value of the dephasing rate to $\gamma_{\text{deph}} = 10^{-1}$ GHz, shown in Fig. 3(b), the oscillatory behavior is lost and the fidelity shows a maximum with low value (≈ 0.55). Finally, for $\gamma_{\text{deph}} = 1$ GHz, shown in Fig. 3(c), the population P_{000} and fidelity decay fast, with P_{111} increasing, until $t \approx 12$ ns, when the density operator becomes a statistical mixture. In fact, for the three dephasing rates considered, it is true

that $\lim_{t \rightarrow \infty} \hat{\rho}(t) = I/8$. This behavior shows that the feasibility of the generation of a GHZ class state in the context of charged qubits is an open experimental challenge, once it is important to guarantee a setup with low values of dephasing rates. Even though we find that the formation of GHZ states in the present system is quite sensitive to charge dephasing, if low dephasing rates are experimentally attained, one can find large fidelity values for both GHZ and FLIP states.

V. SUMMARY

In this work, we discuss the generation of genuine multipartite states belonging to the GHZ class, in the context of semiconductors quantum dots. We encode three qubits in three pairs of charged quantum dots, each pair defining a quantum molecule. In the Coulomb blockade regime, a single electron can be injected in each pair of quantum dots. This excess electron jumps back and forth between the dots, thus encoding a qubit. Electrostatic interaction between the quantum molecules guarantees the coupling between qubits.

We demonstrate that the unitary dynamics of this system can be manipulated to generate states of the GHZ class at short times, considering resonance of the electronic energies and equal values of tunneling rates. Depending on the setup of the initial state, it is possible to create a GHZ or a FLIP state, where the time of formation can be controlled by the value of tunneling coupling. Although this time decreases as the tunneling rate increases, the dynamic shows that high values of Δ are not convenient for the formation of the entangled state, once the dynamics starts to populate other electronic states. Our analytical work permits us to understand the origins of an effective two-level dynamics based on a third-order tunneling process, with the earlier time of formation of a GHZ-class being $\approx \frac{\pi\hbar J^2}{4\Delta^3}$. We simulate the action of charge dephasing, experimentally pointed out as the main mechanism of decoherence in charged quantum molecules. Although the formation of GHZ states can be a challenge due to the dephasing mechanism, the time of formation of the quantum state depends directly on the tunneling parameter, providing a fine control (through gate voltages) that could overcome the time scale of dephasing, by setting a shorter time scale for dynamics.

VI. ACKNOWLEDGMENTS

L.S. thanks Augusto M. Alcalde for the assistance with numerical calculations. This work was supported by CAPES, and the Brazilian National Institute of Science and Technology of Quantum Information (INCT-IQ), grant 465469/2014-0/CNPq.

Appendix A: Generation of the FLIP states

This appendix is devoted to present our results for the generation of the FLIP states, following the same procedure discussed in Sec. III but considering the initial condition $\hat{\rho}(0) = |010\rangle\langle 010|$, and the fidelity target states being $\hat{\rho}_{\text{FLIP}}(\pm\pi/2)$. In Fig. 4, we plot our results for populations, fidelities, and τ_3 , panels below, considering $\Delta = J/6$, the same value of Fig. 2.

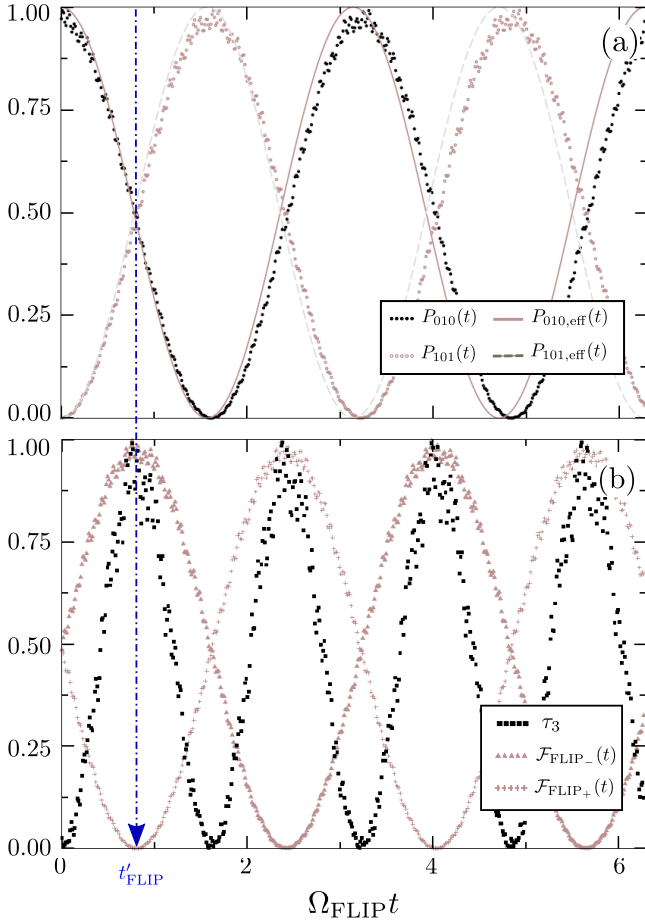


FIG. 4. (Color online) Quantum dynamics against $\Omega_{\text{FLIP}} t$ considering the initial condition $\hat{\rho}(0) = |010\rangle\langle 010|$ for $\varepsilon_i = 0$, $J = 25\mu\text{eV}$ and $\Delta = J/6$. Panel (a): Populations $P_{010}(t)$ (black dots) and $P_{101}(t)$ (brown open circles) and the dynamics of the effective two-level system for the population $P_{010,\text{eff}}(t)$ (brown solid line) and $P_{101,\text{eff}}(t)$ (gray dashed line). Panel (b): Evolution of τ_3 (black squares), and the fidelities $\mathcal{F}_{\text{FLIP}-}(t)$ (brown filled triangles), and $\mathcal{F}_{\text{FLIP}+}(t)$ (brown crosses). Fidelities are calculated using the Eq.(7) for the target states $|\Psi_{\text{FLIP}}(-\pi/2)\rangle$ and $|\Psi_{\text{FLIP}}(\pi/2)\rangle$, respectively. The blue dashed-dot line shows the time of formation of the first GHZ state, corresponding to $t'_{\text{FLIP}} \approx 4.56$ ns.

By comparing this results with those discussed in the main text, we observe a similar behavior for populations, entanglement degree, and fidelities with the main difference being that the dynamically accessed populations are now P_{010} and P_{101} . The fidelity calculations and

τ_3 show that the state $|\Psi_{\text{FLIP}}(-\pi/2)\rangle$ is generated at $t'_{\text{FLIP}} = t'_{\text{GHZ}}$. The continuous lines in panel (a) show the results of the effective two-level model, which coupling parameter is obtained following a similar process that those discussed on Sec. III for the GHZ state.

Appendix B: Characteristics of the energy spectrum and the eigenstates of the three-qubit Hamiltonian

In this appendix, we discuss considerations about the spectrum and eigenstates of the three-qubit system, described by Hamiltonian in Eq. (4). Let us begin by writing the expressions for the diagonal terms of this Hamiltonian, which becomes the terms of hamiltonian \hat{H}_0 in Eq.(15):

$$\begin{aligned} E_{000}^0 &= \varepsilon_1 + \varepsilon_2 + \varepsilon_3 + J_{12} + J_{23}, \\ E_{001}^0 &= \varepsilon_1 + \varepsilon_2 - \varepsilon_3 + J_{12} - J_{23}, \\ E_{010}^0 &= \varepsilon_1 - \varepsilon_2 + \varepsilon_3 - J_{12} - J_{23}, \\ E_{011}^0 &= \varepsilon_1 - \varepsilon_2 - \varepsilon_3 - J_{12} + J_{23}, \\ E_{100}^0 &= -\varepsilon_1 + \varepsilon_2 + \varepsilon_3 - J_{12} + J_{23}, \\ E_{101}^0 &= -\varepsilon_1 + \varepsilon_2 - \varepsilon_3 - J_{12} - J_{23}, \\ E_{110}^0 &= -\varepsilon_1 - \varepsilon_2 + \varepsilon_3 + J_{12} - J_{23}, \\ E_{111}^0 &= -\varepsilon_1 - \varepsilon_2 - \varepsilon_3 + J_{12} + J_{23}. \end{aligned} \quad (\text{B1})$$

If we impose the condition of equal value for detunings, i.e. $\varepsilon_i = 0$, and if the Coulomb coupling is given by $J_{12} = J_{23} = J$, we obtain three different values given by $E = -2J, 0, 2J$. That means, under this particular choice of physical parameters, the spectrum of \hat{H}_0 shows energy degeneracy that permit the definition of three different subspaces:

- $\mathcal{H}_{E=2J}$ with degeneracy 2, which eigenstates are given by $\{|000\rangle, |111\rangle\}$;
- $\mathcal{H}_{E=0}$ with degeneracy 4, which elements are given by $\{|001\rangle, |011\rangle, |100\rangle, |110\rangle\}$;
- $\mathcal{H}_{E=-2J}$ with degeneracy 2 and eigenstates being $\{|010\rangle, |101\rangle\}$.

At this point, we introduce the action of the tunneling, which corresponds to include the nondiagonal terms described by operator \hat{V} , Eq.(20). In Fig. 5(a) we plot the energy spectrum for $J = 25\mu\text{eV}$ against Δ , considering $\Delta = (0, J]$. The energies are written in units of J for the sake of clarity. The action of the tunneling is behind the emergence of anticrossings with the subsequent removal of degeneracy inside each subspace, which becomes important for values above $\Delta = J/2$.

At this point, we search for highly entangled eigenstates, as in previous works [22, 24], connected with anticrossings observed on the energy spectrum. For the

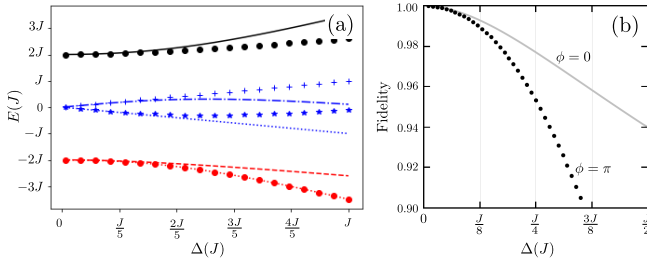


FIG. 5. (Color online) Panel (a): the energy spectrum of the three-qubit Hamiltonian, Eq. (4), against the tunneling coupling Δ considering $J = 25\mu\text{eV}$, $\varepsilon_i = 0$, and equal tunneling rates for the three quantum molecules. The values of energies and Δ are expressed in terms of J . The plot includes the ground state (red circles and dotted line), and the first excited state (red dashed line), originally from the $\mathcal{H}_{E=-2J}$ subspace; the 2nd (blue dotted line), 3rd (blue stars), 4th (blue dot-dashed line), and 5th (blue crosses) excited states, originally from the $\mathcal{H}_{E=0}$ subspace; and finally the 6th (black circles) and 7th (grey solid line) excited states, associated with the $\mathcal{H}_{E=2J}$ subspace. Panel (b): calculation of the fidelity of the states in subspace $\mathcal{H}_{E=2J}$ considering $|\Psi_{\text{GHZ}}(\pi)\rangle$ as the target state for the 6th excited state and $|\Psi_{\text{GHZ}}(0)\rangle$ as the target state for the 7th excited state. Line and symbols are the same used for the corresponding eigenvalues in panel (a).

subspace $\mathcal{H}_{E=2J}$, we seek for eigenstates given by

$$|\Psi_{\text{GHZ}}(0)\rangle = \frac{1}{\sqrt{2}} (|000\rangle + |111\rangle), \quad (\text{B2})$$

$$|\Psi_{\text{GHZ}}(\pi)\rangle = \frac{1}{\sqrt{2}} (|000\rangle - |111\rangle).$$

We proceed to calculate the fidelity of the eigenstates which emerges from subspace $\mathcal{H}_{E=2J}$ considering values for tunneling coupling so $\Delta < J/2$. The results are shown in Fig.5(b), where the high value for the fidelity, above 0.9, corroborates that the eigenstates with the highest energies are approximately $|\Psi_{\text{GHZ}}(0)\rangle$ and $|\Psi_{\text{GHZ}}(\pi)\rangle$, although the fidelity decreases from 0.98 to ≈ 0.90 as Δ increases. A similar result (not shown here) for the fidelities of the ground and first excited states, using as target states $|\Psi_{\text{FLIP}}(\pi)\rangle$ and $|\Psi_{\text{FLIP}}(0)\rangle$ respectively. This results give us confidence to search of a effective two-level model to describe the dynamics behind the formation of the GHZ states, considering the action of tunneling as a perturbation.

Appendix C: The nonlinear effect of the tunneling process and the two-level effective model.

Once the analysis of the spectrum and eigenstates successfully points out the emergence of a well separate two-level system where the states $|000\rangle$ and $|111\rangle$ are coupled by tunneling considered as a perturbation, we are ready to understand the underlying processes behind the formation of the GHZ state. We first split $\mathcal{H}_{3\text{qb}}$ into

two parts, where A contains the eigenstates of \hat{H}_0 , being $\{|000\rangle, |111\rangle\}$ and a segment B containing all the remaining states of the computational basis. We further reorganize the Hilbert space into these two blocks. A state in this new format is represented as

$$|\psi\rangle = \begin{pmatrix} C_A \\ C_B \end{pmatrix}, \quad (\text{C1})$$

where C_A is a 2×1 vector of $|\psi\rangle$ with components in the A subspace, and C_B is a 6×1 vector related with the B subspace. Operators also has an associated block representation in this format. For an operator O given by

$$\hat{O} = \begin{pmatrix} \hat{O}^{AA} & \hat{O}^{AB} \\ \hat{O}^{BA} & \hat{O}^{BB} \end{pmatrix}. \quad (\text{C2})$$

In this case, \hat{O}^{AA} is a 2×2 matrix in the A subspace and \hat{O}^{BB} is a 6×6 matrix. The coupling between A and B is given by \hat{O}^{AB} , a 2×6 operator, and \hat{O}^{BA} , a 6×2 matrix.

Following this definition, we consider $\tilde{H} = \hat{O}$ acting over $|\psi\rangle$ in Eq. C1, obtaining the following system of coupled equations

$$\begin{aligned} \tilde{H}^{AA}C_A + \tilde{H}^{AB}C_B &= EC_A \\ \tilde{H}^{BA}C_A + \tilde{H}^{BB}C_B &= EC_B \end{aligned} \quad (\text{C3})$$

Isolating C_B from the second line above, and replacing in the first line, we obtain

$$\{\tilde{H}^{AA} + \tilde{H}^{AB}(E - \tilde{H}^{BB})^{-1}\tilde{H}^{BA}\}C_A = EC_A. \quad (\text{C4})$$

Note that Eq. (C4) describes the effective dynamics in subspace A where

$$\tilde{H}_{\text{eff}}^{\text{GHZ}} = \tilde{H}^{AA} + \tilde{H}^{AB}(E - \tilde{H}^{BB})^{-1}\tilde{H}^{BA}, \quad (\text{C5})$$

is the effective Hamiltonian operator.

At this point, we define

$$\Omega_{\text{GHZ}} = \langle 111 | \tilde{H}_{\text{eff}}^{\text{GHZ}} | 000 \rangle, \quad (\text{C6})$$

which means the problem of calculate the effective coupling behind the formation of the GHZ states becomes the problem of computing the expression above, considering $\Delta \ll J$.

To begin the calculation, we start with finding the explicit form of the operators \tilde{H}^{AA} , \tilde{H}^{AB} , \tilde{H}^{BA} , \tilde{H}^{BB} . By defining the projector operators P and Q , such that

$$\begin{aligned} \hat{P} &= |000\rangle\langle 000| + |111\rangle\langle 111|, \\ \hat{Q} &= I - \hat{P}, \end{aligned} \quad (\text{C7})$$

where I stands for the identity operator. Using the definitions for \hat{H}_0 and \hat{V} , Eq. (15) and Eq. (19), we obtain

$$\begin{aligned} \tilde{H}^{AA} &= \hat{P}(\hat{H}_0 + \hat{V})\hat{P}, \\ \tilde{H}^{BB} &= \hat{Q}(\hat{H}_0 + \hat{V})\hat{Q}, \\ \tilde{H}^{AB} &= \hat{P}(\hat{H}_0 + \hat{V})\hat{Q}, \\ \tilde{H}^{BA} &= \hat{Q}(\hat{H}_0 + \hat{V})\hat{P}. \end{aligned}$$

Here the operators \tilde{H}^{AA} and \tilde{H}^{BB} are diagonal matrizes, while \tilde{H}^{AB} and \tilde{H}^{BA} are nondiagonal, depending only of the parameter Δ . Substituting Eq. (C5) into Eq. (C6) leave us with

$$\Omega_{\text{GHZ}} = \langle 111 | \tilde{H}^{AB} (E - \tilde{H}^{BB})^{-1} \tilde{H}^{BA} | 000 \rangle, \quad (\text{C8})$$

where we used the fact that \tilde{H}^{AA} is diagonal in A . Using the second line in Eq.(C8), we have

$$\tilde{H}^{BB} = \hat{Q} \tilde{H}_0 \hat{Q} + \hat{Q} \hat{V} \hat{Q} \equiv \tilde{H}_0^{BB} + \hat{V}^{BB}. \quad (\text{C9})$$

Using Eq. (C9) we can write

$$E - \tilde{H}^{BB} = (E - \tilde{H}_0^{BB}) (I - (E - \tilde{H}_0^{BB})^{-1} \hat{V}^{BB}), \quad (\text{C10})$$

and thus it follows the identity

$$(E - \tilde{H}^{BB})^{-1} = \{I - (E - \tilde{H}_0^{BB})^{-1} \hat{V}^{BB}\}^{-1} (E - \tilde{H}_0^{BB})^{-1}. \quad (\text{C11})$$

Substituting (C11) into eq. (C8), we have

$$\begin{aligned} \Omega_{\text{GHZ}} = & \langle 111 | \tilde{H}^{AB} \{I - (E - \tilde{H}_0^{BB})^{-1} \hat{V}^{BB}\}^{-1} \\ & \times (E - \tilde{H}_0^{BB})^{-1} \tilde{H}^{BA} | 000 \rangle. \end{aligned} \quad (\text{C12})$$

At this point, we substitute the operator $\{I - (E - \tilde{H}_0^{BB})^{-1} \hat{V}^{BB}\}^{-1}$ for a Taylor expansion written as

$$\{I - (E - \tilde{H}_0^{BB})^{-1} \hat{V}^{BB}\}^{-1} = I + (E - \tilde{H}_0^{BB})^{-1} \hat{V}^{BB},$$

which is valid for Δ small if compared with the Coulomb coupling J . By substituting this term in the definition of Ω_{GHZ} and inserting two identity operators we obtain Eq (22) from the main text. Notice that one can follow the same procedure to determine Ω_{FLIP} by changing the segment A for the subspace with $E = -2J$, with elements $\{|101\rangle$, and $|101\rangle\}$.

[1] D. Loss and D. P. DiVincenzo, Phys. Rev. A **57**, 120 (1998).
[2] G. Burkard, D. Loss, and D. P. DiVincenzo, Phys. Rev. B **59**, 2070 (1999).
[3] D. M. Zajac, A. J. Sigillito, M. Russ, F. Borjans, J. M. Taylor, G. Burkard, and J. R. Petta, Science **359**, 439 (2018).
[4] Y. He, S. K. Gorman, D. Keith, L. Kranz, J. G. Keizer, and M. Y. Simmons, Nature **571**, 371 (2019).
[5] J. Yoneda, K. Takeda, T. Otsuka, T. Nakajima, M. R. Delbecq, G. Allison, T. Honda, T. Kodera, S. Oda, Y. Hoshi, *et al.*, Nature Nanotechnology **13**, 102 (2018).
[6] T. Hayashi, T. Fujisawa, H. D. Cheong, Y. H. Jeong, and Y. Hirayama, Phys. Rev. Lett. **91**, 226804 (2003).
[7] G. Shinkai, T. Hayashi, T. Ota, and T. Fujisawa, Phys. Rev. Lett. **103**, 056802 (2009).
[8] J. R. Petta, A. C. Johnson, J. M. Taylor, E. A. Laird, A. Yacoby, M. D. Lukin, C. M. Marcus, M. P. Hanson, and A. C. Gossard, Science **309**, 2180 (2005).
[9] J. M. Nichol, L. A. Orona, S. P. Harvey, S. Fallahi, G. C. Gardner, M. J. Manfra, and A. Yacoby, npj Quantum Information **3**, 3 (2017).
[10] E. A. Laird, J. M. Taylor, D. P. DiVincenzo, C. M. Marcus, M. P. Hanson, and A. C. Gossard, Phys. Rev. B **82**, 075403 (2010).
[11] R. Ashoori, Nature **379**, 413 (1996).
[12] E. Schöll, L. Hanschke, L. Schweikert, K. D. Zeuner, M. Reindl, S. F. Covre da Silva, T. Lettner, R. Trotta, J. J. Finley, K. Müller, A. Rastelli, V. Zwiller, and K. D. Jöns, Nano Lett. **19**, 2404 (2019).
[13] H. Borges, L. Sanz, and A. Alcalde, Physics Letters A **380**, 3111 (2016).
[14] H. S. Borges, L. Sanz, J. M. Villas-Bôas, O. O. Diniz Neto, and A. M. Alcalde, Phys. Rev. B **85**, 115425 (2012).
[15] M. Russ, D. M. Zajac, A. J. Sigillito, F. Borjans, J. M. Taylor, J. R. Petta, and G. Burkard, Phys. Rev. B **97**, 085421 (2018).
[16] S. Bugu, F. Ozaydin, T. Ferrus, and T. Kodera, Scientific Reports **10**, 1 (2020).
[17] H. Kiyama, A. Korsch, N. Nagai, Y. Kanai, K. Matsumoto, K. Hirakawa, and A. Oiwa, Scientific Reports **8**, 13188 (2018).
[18] J. Park, A. N. Pasupathy, J. I. Goldsmith, C. Chang, Y. Yaish, J. R. Petta, M. Rinkoski, J. P. Sethna, H. D. Abrúñia, M. P. L., and D. C. Ralph, Nature **417**, 722 (2002).
[19] G. Shinkai, T. Hayashi, Y. Hirayama, and T. Fujisawa, Appl. Phys. Lett. **90**, 103116 (2007).
[20] D. Xiang, X. Wang, C. Jia, T. Lee, and X. Guo, Chem. Rev. **116**, 4318 (2016).
[21] Y. Xue and M. A. Ratner, International Journal of Quantum Chemistry **102**, 911 (2005).
[22] F. M. Souza, P. A. Oliveira, and L. Sanz, Phys. Rev. A **100**, 042309 (2019).
[23] F. M. Souza and L. Sanz, Physical Review A **96**, 052110 (2017).
[24] P. Oliveira and L. Sanz, Ann. Physics **356**, 244 (2015).
[25] V. M. Stojanović, Physical Review Letters **124**, 190504 (2020).
[26] T. Fujisawa, G. Shinkai, T. Hayashi, and T. Ota, Phys. E **43**, 730734 (2011).
[27] T. Fujisawa, T. H. Oosterkamp, W. G. van der Wiel, B. W. Broer, R. Aguado, S. Tarucha, and L. P. Kouwenhoven, Science **282**, 932 (1998).
[28] I. Ka, V. Le Borgne, K. Fujisawa, T. Hayashi, Y. A. Kim, M. Endo, D. Ma, and M. A. El Khakani, Materials Today Energy **16**, 100378 (2020).
[29] L. P. Kouwenhoven, N. C. Van der Vaart, A. Johnson, W. Kool, C. Harmans, J. Williamson, A. Staring, and C. Foxon, Zeitschrift für Physik B Condensed Matter **85**, 367 (1991).
[30] R. Horodecki, P. Horodecki, M. Horodecki, and K. Horodecki, Rev. Mod. Phys. **81**, 865 (2009).

- [31] W. Dur, G. Vidal, and J. I. Cirac, Phys. Rev. A **62**, 062314 (2000).
- [32] C. Sabin and G. Alcaine, The European Physical Journal D **48**, 435 (2008).
- [33] V. Coffman, J. Kundu, and W. K. Wootters, Phys. Rev. A **61**, 052306 (2000).
- [34] The quantity τ_2 is zero, although becomes non negligible for $\Delta > J/4$.
- [35] X. Zhang, H.-O. Li, G. Cao, M. Xiao, G.-C. Guo, and G.-P. Guo, National Science Review **6**, 32 (2018).
- [36] M. Nielsen, *Quantum Computation and Quantum Information*, 1st ed. (Cambridge University Press, Cambridge, 2010).
- [37] M. M. Wilde, *Quantum Information Theory*, 2nd ed. (Cambridge University Press, Cambridge, 2017).